

Influence of character of carrier reflection on the doppleron oscillations in metals with open orbits

I. F. Voloshin, N. A. Podlevskikh, V. G. Skobov, L. M. Fisher, and A. S. Chernov

V. I. Lenin All-Union Electrotechnical Institute

(Submitted 17 February 1983)

Zh. Eksp. Teor. Fiz. **85**, 373–386 (July 1983)

The impedance oscillations of a compensated metal in the presence of open orbits are investigated theoretically and experimentally. The theoretical analysis is carried for a simple Fermi-surface model for which an exact analytic solution of the integrodifferential equation for the RF field in the metal can be obtained at an arbitrary value of the Fuchs specularity parameter. The skin-effect components corresponding to the electric-field components along and across trajectories have different penetration depths. As a result, in nonspecular scattering of the electrons the amplitudes of the doppleron oscillations for the various diagonal impedance-tensor components are different, even though the doppleron modes themselves have circular polarization. The impedances of single-crystal cadmium and silver plates whose normals are parallel to the binary axes are studied experimentally. The measurements are performed in a magnetic field perpendicular to the plate surfaces. In cadmium plates, the impedance oscillations due to Doppler-shifted cyclotron resonance are observed predominantly for one of the linear polarizations of the exciting field. Helicon oscillations in silver are observed for both negative and positive circular polarization, although the amplitude of the latter is significantly lower. The experimental results are in agreement with the conclusions of the theory developed here.

PACS numbers: 73.25. + i, 76.40. + b

The skin effect and the Doppler-shifted cyclotron resonance (DSCR) were investigated¹ in metals with open orbits in the case of specular carrier reflection from the surface. It was shown, in particular, that the presence of open orbits does not alter the polarization of the doppleron oscillations: when a plate is excited by a linearly polarized field the amplitude of the oscillations does not depend on the orientation of this field in the sample plane. It was demonstrated in Ref. 2 that in the case of diffuse scattering the open orbits can alter substantially the amplitude and polarization of the oscillations. In the present study we have investigated the influence of open orbits on the impedance oscillations of a plate at an arbitrary value of the specularity coefficient p . The presence of open trajectories increases the conductivity in the corresponding direction, and this decreases the depth of penetration of the skin-effect component whose electric field is parallel to these trajectories. Under conditions of nonspecular carrier reflection this makes the amplitude of the doppleron oscillations much smaller if the exciting electric field is oriented along the open trajectories. The same is valid also for the Gantmakher-Kaner oscillations. This effect is of particular importance for compensated metals, in which impedance oscillations are observed in a wide range of magnetic fields.

1. THEORY

1. We derive an equation for the distribution of the electric field in a metal plate at arbitrary p . In the case of an unbounded metal the current density j in the equation for monochromatic waves of frequency ω

$$\frac{d^2 \mathcal{E}(z)}{dz^2} = -\frac{4\pi i \omega}{c^2} j(z), \quad (1)$$

is given by the expression

$$j_\alpha(z) = \int_{-\infty}^{\infty} \sigma_{\alpha\beta}(z-z') \mathcal{E}_\beta(z') dz',$$

where \mathcal{E} is the electric-field intensity, $\sigma_{\alpha\beta}$ is the nonlocal-conductivity tensor, and z is the coordinate along the propagation vector k .

Let the constant magnetic field H be parallel to the vector k and assume that on the carrier trajectories there are no points at which the velocity component v_z reverses sign. Then $\sigma_{\alpha\beta}$ depends only on the projection of the electron path on the z axis.

We consider now a plate $0 \leq z \leq d$. The current density j inside the plate is determined both by the electrons reaching directly the point z from the point z' , and by electrons that are reflected in their path from the plate surface. The contribution of electrons that negotiate a path Δ as they move from the point z' to the point z and experience n reflections from the plate surfaces is equal to

$$p^n \int_0^d \sigma_{\alpha\beta}(\Delta(z, z')) \mathcal{E}_\beta(z') dz',$$

where p is the probability of specular reflection. Summing the contributions of all the electrons we find

$$j_\alpha(z) = \int_0^d \left[\sum_{h=-\infty}^{\infty} \sigma(z-z'-2kd) p^{|2h-1|} + \sum_{h=-\infty}^{\infty} \sigma(z+z'-2kd) p^{|2h-1|} \right] \mathcal{E}(z') dz'. \quad (2)$$

We consider antisymmetrical excitation of a plate, wherein $\mathcal{E}_\alpha(d-z) = -\mathcal{E}_\alpha(z)$. In this case it is convenient to make in the second sum of (2) the substitution $z' \rightarrow d-z''$ and combine the two sums. Substituting next in (1) the expression for j_α we obtain the equation

$$\frac{d^2 \mathcal{E}_\alpha(z)}{dz^2} + \frac{4\pi i \omega}{c^2} \int_0^d \sum_{n=-\infty}^{\infty} \sigma_{\alpha\beta}(z-z'-nd) (-p)^{|n|} \mathcal{E}_\beta(z') dz' \quad (0 \leq z \leq d). \quad (3)$$

2. In a constant magnetic field \mathbf{H} perpendicular to the plate surface, Eq. (3) takes in dimensionless variables the form

$$\frac{d^2 \mathcal{E}_\alpha(\xi)}{d\xi^2} + i\xi \int_0^L \sum_{n=-\infty}^{\infty} (-p)^{|n|} s_{\alpha\beta}(\xi-\xi'-nL) \mathcal{E}_\beta(\xi') d\xi' = 0 \quad (\alpha, \beta = x, y), \quad (4)$$

where

$$\xi = \frac{2\pi z}{u}, \quad L = \frac{2\pi d}{u}, \quad u = \frac{c}{eH} \left(\frac{\partial S}{\partial p_z} \right)_{\max}, \quad (5)$$

$$\xi = \frac{\omega N_1 e u^2}{\pi c H}, \quad s_{\alpha\beta}(\xi) = \frac{H}{N_1 e c} \sigma_{\alpha\beta}(\xi), \quad (6)$$

u is the maximum displacement of the electrons during the cyclotron period, $\partial S / \partial p_z$ is the derivative of the area of intersection of the Fermi surface with the plane $p_z = \text{const}$, p_z is the projection of the momentum on the magnetic-field direction, and N_1 is the electron density.

We shall use a model² in which the electron Fermi surface is a parabolic lens whose axis is parallel to p_z , and the Fermi hole surface is a cylinder parallel to p_z . The section of the cylinder in the $p_y p_z$ plane is made up of two parabolas inverted counter to each other, with vertices on the p_z axis. In this model the longitudinal velocities of the electrons are equal to $\pm v_1$, the longitudinal velocities of the holes are equal to $\pm v_2$, and the transverse velocities of the holes are directed along the y axis. For purposes of compensation we introduce also local holes whose Fermi surface is a circular cylinder with axis parallel to p_z .

The tensor $s_{\alpha\beta}(\xi)$ is defined by its Fourier components,

$$s_{\alpha\beta}(\xi) = \frac{1}{2\pi} \int_{-\infty}^{\infty} s_{\alpha\beta}(q) e^{iq\xi} dq, \quad (7)$$

which take in our model the form

$$s_{xx}(q) = \frac{i}{2} \left[\frac{1+i\gamma_1}{(1+i\gamma_1)^2 - q^2} - \frac{1-i\gamma_1}{(1-i\gamma_1)^2 - q^2} \right], \quad (8)$$

$$s_{yz}(q) = -s_{xy}(q) = \frac{1}{2} \left[\frac{1+i\gamma_1}{(1+i\gamma_1)^2 - q^2} + \frac{1-i\gamma_1}{(1-i\gamma_1)^2 - q^2} \right] - (1-\mu), \quad (9)$$

$$s_{yy}(q) = s_{zz}(q) + s_0(q), \quad s_0(q) = \frac{\eta\gamma}{\gamma^2 + q^2}, \quad (10)$$

where

$$\mu = \frac{N_2}{N_1}, \quad \eta = \mu \frac{m_1 v_1}{m_2 v_2}, \quad \gamma_1 = \frac{u}{2\pi} \frac{v_1}{v_1}, \quad \gamma = \frac{u}{2\pi} \frac{v_2}{v_2}, \quad u = 2\pi \frac{m_1 v_1 c}{eH}, \quad (11)$$

$N_{1,2}, m_{1,2}$ and $v_{1,2}$ are the densities, masses and collision frequencies and of the holes having open orbits. We have taken into account the Hall conductivity $1 - \mu$ of the local holes, but neglected their collisions and the corresponding corrections to the conductivity. The term s_0 in s_{yy} is the contribution of the holes with open orbits.

3. In circular polarizations $\mathcal{E}_\pm = \mathcal{E}_x \pm i\mathcal{E}_y$, $s_\pm = s_{xx} \pm is_{yx}$ the system (4) takes the form

$$\begin{aligned} & \frac{d^2 \mathcal{E}_+}{d\xi^2} + i\xi \int_0^L \{ V_+(\xi-\xi') \mathcal{E}_+(\xi') \\ & + \frac{1}{2} V_0(\xi-\xi') [\mathcal{E}_+(\xi') - \mathcal{E}_-(\xi')] \} d\xi' = 0, \\ & \frac{d^2 \mathcal{E}_-}{d\xi^2} + i\xi \int_0^L \{ V_-(\xi-\xi') \mathcal{E}_-(\xi') \\ & - \frac{1}{2} V_0(\xi-\xi') [\mathcal{E}_+(\xi') - \mathcal{E}_-(\xi')] \} d\xi' = 0, \end{aligned} \quad (12)$$

where

$$V(\xi) = \sum_{n=-\infty}^{\infty} (-p)^{|n|} s(\xi-nL). \quad (13)$$

In our model, the Fourier components $s_{\alpha\beta}(q)$ of the conductivity have only simple poles in the complex q plane. The integrals in (7) are expressed therefore in terms of exponentials, and the series in (13) can be easily summed. By way of example we present the expression for V_+ :

$$V_+(\xi) = \frac{1}{2} \left\{ e^{i(1+i\gamma_1)|\xi|} - \frac{p e^{i(1+i\gamma_1)L}}{1+p e^{i(1+i\gamma_1)L}} [e^{i(1+i\gamma_1)\xi} + e^{-i(1+i\gamma_1)\xi}] \right\} - i(1-\mu) \delta(\xi). \quad (14)$$

From (14) it follows that

$$\left[\frac{d^2}{d\xi^2} + (1+i\gamma_1)^2 \right] \int_0^L \{ V_+(\xi-\xi') + i(1-\mu) \delta(\xi-\xi') \} \mathcal{E}_+(\xi') d\xi' = i(1+i\gamma_1) \mathcal{E}_+(\xi). \quad (15)$$

Applying the differentiation operator to Eqs. (12), taking their linear combinations, and using relations of the type (15), we transform the system of integrodifferential equations into a system of two differential equations (of fourth and sixth order) with constant coefficients. These equations describe the natural modes of the electromagnetic field in an unbounded metal, and accordingly do not contain p and L . They have only exponential solutions. We seek a general solution, antisymmetric about the point $\xi = L/2$, in the form

$$\begin{aligned} \mathcal{E}_+(\xi) &= \sum_{n=1}^5 a_n [e^{iq_n \xi} - e^{iq_n(L-\xi)}], \\ \mathcal{E}_-(\xi) &= \sum_{n=1}^5 b_n [e^{iq_n \xi} - e^{iq_n(L-\xi)}]. \end{aligned} \quad (16)$$

Substituting (16) in the differential equations, we obtain the characteristic (dispersion) equation

$$[q^2 - i\xi s_+(q)] [q^2 - i\xi s_-(q)] - i\xi s_0(q) [q^2 - i\xi s_{xx}(q)] = 0, \quad (17)$$

which defines the wave vectors $k_n = 2\pi q_n / u$ ($\text{Im } q_n > 0$) of the different modes, and the algebraic equations

$$A_n a_n + B_n b_n = 0 \quad (n=1, 2, 3, 4, 5), \quad (18)$$

$$A_n = [\gamma^2 + (1 - i\gamma_1)^2] \{ [q_n^2 - (1 - \mu)\xi] [(1 + i\gamma_1)^2 - q_n^2] + \xi(1 + i\gamma_1) \} + 2\eta\gamma\gamma_1\xi, \quad (19)$$

$$B_n = [\gamma^2 + (1 + i\gamma_1)^2] \{ [q_n^2 + (1 - \mu)\xi] [(1 - i\gamma_1)^2 - q_n^2] - \xi(1 - i\gamma_1) \} - 2\eta\gamma\gamma_1\xi,$$

which determine their polarization.

As a result of substitution of (16) in (12) the integrals in (12) are expressed not only in terms of the exponentials $\exp(\pm iq_n \zeta)$ but also in terms of $\exp[\pm i(1 + i\gamma_1)\zeta]$, $\exp[\pm i(1 - i\gamma_1)\zeta]$, and $\exp(\pm \gamma \zeta)$. From the condition that there be no such terms in the current we get three algebraic equations for the coefficients a_n and b_n . Even though the coefficients in the kernels V in (12) contain the quantities $\exp[\pm i(1 \pm i\gamma_1)L]$ and $\exp(-\gamma L)$, the equations for a_n and b_n do not contain these quantities. Finally, two boundary conditions imposed on \mathcal{E}_+ and \mathcal{E}_- on one of the surfaces of the plate yield two more equations. The result is a system of ten linear algebraic equations for the ten unknowns a_n and b_n . Introducing the notation

$$c_n = \frac{q_n}{2} (1 + e^{iq_n L}) (a_n + b_n), \quad d_n = \frac{q_n}{2} (1 + e^{iq_n L}) (a_n - b_n), \quad (20)$$

$$\lambda = \frac{1-p}{1+p}, \quad t_n = \frac{1 - e^{iq_n L}}{q_n (1 + e^{iq_n L})}, \quad (21)$$

we write this system in the form

$$\sum_{n=1}^5 \frac{c_n + d_n}{q_n^2 - (1 + i\gamma_1)^2} [1 + \lambda(1 + i\gamma_1)t_n] = 0, \quad (22)$$

$$\sum_{n=1}^5 \frac{c_n - d_n}{q_n^2 - (1 - i\gamma_1)^2} [1 - \lambda(1 - i\gamma_1)t_n] = 0,$$

$$\sum_{n=1}^5 \frac{d_n}{q_n^2 + \gamma^2} (1 + i\lambda\gamma t_n) = 0,$$

$$\sum_{n=1}^5 c_n = -i\mathcal{E}'_x(0), \quad \sum_{n=1}^5 d_n = \mathcal{E}'_y(0), \quad (23)$$

$$d_n = J_n c_n \quad (n=1, 2, 3, 4, 5),$$

where $\mathcal{E}'(0) = (d\mathcal{E}/d\zeta)_{\zeta=0}$,

$$J_n = \frac{B_n + A_n}{B_n - A_n}. \quad (24)$$

The elements of the plate impedance tensor $Z_{\alpha\beta}$ are expressed in terms of the coefficient c_n and d_n by means of the equations

$$aZ_{x\beta}\mathcal{E}'_{\beta}(0) = i\mathcal{E}'_x(0) = i \sum_{n=1}^5 t_n c_n, \quad (25)$$

$$aZ_{y\beta}\mathcal{E}'_{\beta}(0) = i\mathcal{E}'_y(0) = \sum_{n=1}^5 t_n d_n,$$

where $a = c^2/4\omega u$.

4. Analysis of the dispersion equation (17) shows that five of its roots with positive imaginary parts are divided into three types. The first comprises the roots (q_4 and q_5) whose values are close to ± 1 in the magnetic-field region where $\xi \ll 1$. The corresponding modes are dopplerons. Substitution of the exact expressions for q_4 and q_5 in (24) yields

$$J_4 = -1, \quad J_5 = 1. \quad (26)$$

This means that the doppleron field q_4 has a "minus" circular polarization, and that of doppleron q_5 a "plus" polarization.

The smallest root, q_3 , is determined by the relation

$$q_3^2 = \frac{i\xi\gamma_1}{1 + \varepsilon^2} \left(1 + \frac{\mu^2\gamma}{\eta\gamma_1} \right), \quad (27)$$

where

$$\varepsilon^2 = \mu^2 \xi / i\eta\gamma. \quad (28)$$

The corresponding modes represent the spin component. Substitution of (27) into the equation for J_3 leads to the expression

$$J_3 = \frac{\mu}{i\eta\gamma} \frac{i\xi\gamma_1 + \gamma^2}{1 + \varepsilon^2}. \quad (29)$$

We shall be interested hereafter in the region with not too weak magnetic fields, in which

$$\gamma_1 \ll \mu. \quad (30)$$

In this region $|J_3| \ll 1$ and consequently $|d_3| \ll |c_3|$, i.e., the electric field of the q_3 mode is polarized predominantly along the x axis.

The roots q_1 and q_2 make up the third type. In the region $\xi \ll 1$ the expressions for them are

$$q_{1,2}^2 = \pm [i\eta\gamma\xi(1 + \varepsilon^2)]^{1/2} + 1/2(1 + \varepsilon^2)(i\xi\gamma_1 + \gamma^2) - \mu\xi^2 - \gamma^2. \quad (31)$$

Substituting (31) in (24) we obtain

$$J_{1,2} = \left(\mp \frac{\varepsilon}{(1 + \varepsilon^2)^{1/2}} - \frac{\xi}{1 + \varepsilon^2} - \frac{1}{2} J_3 \right)^{-1}. \quad (32)$$

The character of the modes 1 and 2 depends on the magnetic field strength. In moderate fields, characterized by the inequality

$$|\varepsilon|^2 \gg 1, \quad (33)$$

we get from (24) the relations

$$J_1 \approx -1, \quad J_2 \approx 1, \quad (34)$$

which are valid also at $\xi \sim 1$. In this region the mode 1, having a minus circular polarization, constitutes a helicon, and the mode 2 with plus polarization, a "damped helicon."

In the region of stronger fields, where

$$|\varepsilon|^2 \ll 1, \quad (35)$$

it follows from (32) that

$$|J_{1,2}| \gg 1 \quad (36)$$

and both modes are polarized along the y axis. Their wave vectors \mathbf{k}_1 and \mathbf{k}_2 are essentially complex and independent of H . Qualitatively these modes have the same character as in the anomalous skin effect.

5. In the region (33) the system (22), (23) is greatly simplified as a result of (26), (24), and the inequality $|J_3| \ll 1$.

Solving this system and using the smallness of q_3 , we write the expressions for the elements of the tensor $Z_{\alpha\beta}$ in the form

$$aZ_{xx} = aZ_{yy} + M = K_1 + L_1 + M, \quad aZ_{xy} = -aZ_{yx} = i(K_2 + L_2), \quad (37)$$

$$K_{1,2} = \frac{1}{2} \left(\frac{\alpha_3 t_2 - \alpha_2 t_3 \pm \beta_4 t_1 - \beta_1 t_4}{\alpha_5 - \alpha_2} \pm \frac{\beta_4 t_1 - \beta_1 t_4}{\beta_4 - \beta_1} \right), \quad (38)$$

$$L_{1,2} = \frac{t_3}{4\varepsilon^2 G \delta_3} (P_+ - P_-) (P_+ \mp P_-), \quad (39)$$

$$M = \frac{t_3}{\varepsilon^2 G \delta_3} P_+ P_-, \quad (40)$$

where

$$G = 1 + \frac{\lambda t_3}{2\varepsilon^2 \delta_3} \left(\frac{q_4^2 - q_1^2}{\beta_4 - \beta_1} - \frac{q_5^2 - q_2^2}{\alpha_5 - \alpha_2} \right), \quad (41)$$

$$P_+ = 1 + \lambda \frac{t_2 - t_3}{\alpha_5 - \alpha_2}, \quad P_- = 1 - \lambda \frac{t_1 - t_4}{\beta_4 - \beta_1}, \quad (42)$$

$$\alpha_n = [1 + \lambda(1 + i\gamma_1)t_n] [(1 + i\gamma_1)^2 - q_n^2]^{-1},$$

$$\beta_n = [1 - \lambda(1 - i\gamma_1)t_n] [(1 - i\gamma_1)^2 - q_n^2]^{-1}, \quad (43)$$

$$\delta_n = 1 + i\lambda\gamma t_3. \quad (44)$$

We note that (39)–(41) do not contain the quantities $\delta_{1,2}$ and $\delta_{4,5}$, since their values differ very little from unity, and we have neglected these differences.

To calculate $Z_{\alpha\beta}$ in the region (35), we represent the quantities c_n in the form

$$c_n = -i\mathcal{E}'_x(0)x_n + \mathcal{E}'_y(0)y_n. \quad (45)$$

Substituting (45) in (22) and (23) and equating to zero the factors of $\mathcal{E}'_x(0)$ and $\mathcal{E}'_y(0)$ in (22), we obtain equations for x_n and y_n . The system of equations for x_n is

$$\sum_{n=1}^5 \alpha_n (1 + J_n) x_n = 0, \quad \sum_{n=1}^5 \beta_n (1 - J_n) x_n = 0, \\ \sum_{n=1}^5 \frac{\delta_n J_n}{q_n^2 + \gamma^2} x_n = 0, \quad \sum_{n=1}^5 x_n = 1, \quad \sum_{n=1}^5 J_n x_n = 0. \quad (46)$$

The system for y_n differs from (46) in that the right-hand sides of the fourth and fifth equations contain zero and unity, respectively.

The elements of the tensor $Z_{\alpha\beta}$ are expressed in terms of x_n and y_n as follows:

$$aZ_{xx} = \sum_{n=1}^5 t_n x_n, \quad aZ_{xy} = i \sum_{n=1}^5 t_n y_n, \quad (47)$$

$$aZ_{yx} = -i \sum_{n=1}^5 t_n J_n x_n, \quad aZ_{yy} = \sum_{n=1}^5 t_n J_n y_n.$$

Using expressions (26), (29), and (32) for J_n and solving the system (46) we obtain

$$x_{1,2} = \frac{1}{J_{1,2}} \left(\frac{f}{h} \mp \frac{1}{2} \varepsilon \delta_3 g \right), \quad x_3 = g, \quad (48)$$

$$x_{4,5} = \frac{1-g}{2} \pm \frac{f}{h},$$

where

$$f = \frac{1}{2} \left(\frac{\alpha_5}{\alpha_5 - \alpha_3} - \frac{\beta_4}{\beta_4 - \beta_3} \right), \quad g = \frac{1}{2} \left(\frac{\alpha_5}{\alpha_5 - \alpha_3} + \frac{\beta_4}{\beta_4 - \beta_3} \right), \quad (49)$$

$$h = 2g - \varphi - \psi, \quad \varphi = \frac{1}{2} \frac{\alpha_1 + \alpha_2}{\alpha_5 - \alpha_3}, \quad \psi = \frac{1}{2} \frac{\beta_1 + \beta_2}{\beta_4 - \beta_3}.$$

Solution of the system of equations for y_n yields

$$y_{1,2} = \frac{g}{h J_{1,2}}, \quad y_3 = f + g \left(\frac{\varphi - \psi}{h} + J_3 + \xi - i\lambda\gamma \varepsilon t_- \right), \quad (50)$$

$$y_{4,5} = \frac{1}{2h} [(f - g \pm 1)\varphi + (f + g \pm 1)\psi], \quad t_{\pm} = \frac{1}{2} (t_1 \pm t_2).$$

6. Expressions (47)–(50), which determine the plate impedance in the field region (35), can be substantially simplified by disregarding the intermediate values of the parameters for which $\lambda\xi|t_3| \sim 1$. At $\lambda\xi|t_3| \gg 1$ we obtain

$$aZ_{xx} = \frac{I}{\lambda\xi}, \quad aZ_{yy} = \frac{I t_+}{I + \lambda\xi t_+}, \quad (51)$$

$$aZ_{xy} = -aZ_{yx} = \frac{i\lambda t_+ (t_4 + t_5)}{2(I + \lambda\xi t_+)},$$

where

$$I = 1 + \frac{1}{2}\lambda(t_5 - t_4). \quad (52)$$

In the opposite case $\lambda\xi|t_3| \ll 1$ we have

$$aZ_{xx} = \left[1 + \frac{1}{2} \left(\frac{\alpha_3}{\alpha_5} + \frac{\beta_3}{\beta_4} \right) \right] t_3 - \frac{1}{2} \left(\frac{\beta_3}{\beta_4} t_4 + \frac{\alpha_3}{\alpha_5} t_5 \right), \\ iaZ_{yx} = J_3 t_3 - \varepsilon \delta_3 \left[1 + \frac{1}{2} \left(\frac{\alpha_3}{\alpha_5} + \frac{\beta_3}{\beta_4} \right) \right] t_- \\ + \frac{1}{2} \left(\frac{\alpha_3}{\alpha_5} - \frac{\beta_3}{\beta_4} \right) t_+ + \frac{1}{2} \left(\frac{\beta_3}{\beta_4} t_4 - \frac{\alpha_3}{\alpha_5} t_5 \right), \\ aZ_{yy} = \left[1 + \frac{1}{4} \left(\frac{\alpha_1 + \alpha_2}{\alpha_5} + \frac{\beta_1 + \beta_2}{\beta_4} \right) \right] t_+ \\ - \frac{1}{4} \left(\frac{\beta_1 + \beta_2}{\beta_4} t_4 + \frac{\alpha_1 + \alpha_2}{\alpha_5} t_5 \right). \quad (53)$$

We shall use the equations derived to describe the behavior of the doppleron oscillations of the impedance of a compensated-metal plate. If the electron reflection is specular, the oscillations of Z_{xx} and Z_{yy} are small and equal in amplitude. For nonspecular reflection they become stronger because of the presence of long-wave skin components of the field.³ In this case, owing to the difference between the skin-effects in the x and y polarizations, the oscillations in the elements Z_{xx} and Z_{yy} are generally speaking enhanced to different degrees. In accordance with Ref. 3, the enhancement of the amplitude of doppleron oscillations in nonspecular reflection is determined by the square of the smooth part

of the plate impedance. For x polarization, the enhancement factor is

$$\left(\xi + \frac{1+\lambda}{\lambda t_3} \right)^{-2}, \quad (54)$$

and for y polarization,

$$\left(\xi + \frac{1+\lambda}{\lambda t_+} \right)^{-2}. \quad (55)$$

We consider the change of the oscillation amplitudes with change of the magnetic field, assuming λ to be fixed. It follows from (54) and (55) that at $\lambda \xi |t_+| \gg 1$ the gain of the oscillations in Z_{xx} and Z_{yy} is the same and equals ξ^{-2} . Therefore the observed impedance oscillations, just as the doppleron modes themselves, have circular polarizations. In the field region where the following inequalities hold

$$|t_3|^{-1} \ll \lambda \xi \ll |t_+|^{-1}, \quad (56)$$

the gain of the oscillations in Z_{yy} , due to the thinner skin layer, is characterized by a factor $|\lambda t_+ / (1 + \lambda)|^2$, which is substantially smaller than the gain of the oscillations in Z_{xx} . As a result, the amplitude of the oscillations in Z_{yy} decreases with increasing H . The ratio of the amplitudes of the oscillations in Z_{yy} and Z_{xx} in the region (56) is of the order of $|\lambda \xi t_+|^2$. Finally, in the region $|\lambda \xi t_3| \ll 1$ the oscillations in Z_{xx} also stop growing with increasing magnetic field and the ratio of the oscillation amplitudes becomes equal to $|t_+ / t_3|^2$.

Thus, although the dopplérons have circular polarization, in the magnetic-field region $|\lambda \xi t_+| \ll 1$ the doppleron oscillation should be observed predominantly in the component Z_{xx} . This is the result of the fact that the presence of open orbits decreases the thickness of the skin layer whose electric field is polarized along the y axis.

Equations (37)–(44) allow us to study the behavior of the impedance oscillations in the region of magnetic fields (33) in which the modes 1 and 2 are helicons. Analysis leads to the following result: the field region in which the oscillations in Z_{yy} become much smaller than in Z_{xx} is determined by the inequality $\lambda \xi |t_1| < 1$ which, as a matter of fact, coincides with the second inequality of (56). In other words, the transition region can be located in the strongest as well as in moderate fields, and is not connected with the character of the modes 1 and 2.

A distinguishing feature of the model considered by us is the absence of branch points in $s_{\pm}(g)$ and accordingly the absence of the Gantmakher-Kaner effect. In the case of more realistic Fermi surfaces, Gantmakher-Kaner oscillations (GKO) exist besides the doppleron oscillations. It is quite obvious that the conclusions drawn above will be qualitatively valid also for these oscillations.

2. EXPERIMENT AND DISCUSSION

We investigated in the experiments the impedance features of cadmium and silver plates in a geometry wherein the Fermi surface has open orbits. In the case of cadmium the constant magnetic field H is oriented near the (0001) plane, and in the case of silver we have $\mathbf{H} \parallel \mathbf{n} \parallel [110]$ (\mathbf{n} is the normal to the plate surface). We have undertaken a detailed study of the oscillations in cadmium not only with an aim at elucidating the role of the open orbits, but also in connection with the

existing contradictions in the interpretation of the nature of the oscillation in the $\mathbf{H} \parallel \mathbf{n} \parallel [11\bar{2}0]$ geometry. Oscillations under these conditions were first observed in Ref. 4 and interpreted as the Gantmakher-Kaner effect. It was shown later in Ref. 5 that at $\mathbf{H} \parallel \mathbf{n} \parallel [11\bar{2}0]$, in fields above a threshold value $H_L \approx 2.5$ kOe/MHz^{1/3}, a doppleron is also excited and is connected with the DSCR of the lens electrons. Since, however, the authors of Ref. 6 did not observe a dependence of the oscillation amplitude on the sign of the circular polarization, they reached the conclusion that there is no doppleron in this geometry. It follows at the same time from the theory developed above that in the presence of open orbits both doppleron oscillations and GKO exist predominantly in one of the linear polarizations. Therefore when the plate is excited by a circularly polarized external field the signal recorded is practically independent of the field-rotation direction, and the use of circular polarization in this case does not permit separation of these two types of oscillation.

1. The impedance measurement procedure is described in Ref. 7. The measurements were made in the frequency range 0.1–1.0 MHz in fields up to 50 kOe at temperatures 1.5–4.2 K. The use of an amplitude bridge permitted a hundred-fold change of the frequency without the need for changing the measurement coil. The cadmium plates, 0.3–1.2 mm thick and of area 4×12 mm, were cut by the electric-spark method from a single crystal with a resistivity ratio $\rho_{300\text{K}} / \rho_{4.2\text{K}} \approx 3 \cdot 10^4$. The normal to each of the plates coincided accurate to 2° with the $[11\bar{2}0]$ or the $[10\bar{1}0]$ axis. The measurements were performed in a linearly polarized electromagnetic field. The direction of the electric field \mathbf{E} in the sample plane could be varied by rotating the coil. The orientation of the field \mathbf{H} along the C_2 axis was determined from the symmetry of the angular dependences of the impedance.

Typical plots of the real and imaginary parts of the particle impedance are shown in Fig. 1. The ordinates are the quantities $R(H) = R(0)$ (a) and $X(H) - X(0)$ (b). The impedance calibration methods are described in Ref. 7. At $f = 510$ kHz the value of $Z(0)$ is approximately $(4\pi/c)(1 - i\sqrt{3}) \cdot 5 \cdot 10^{-8}$. Curves 1 correspond to the polarization $\mathbf{E} \parallel C_6$, at which the current is perpendicular to the direction of the open trajectories, while curves 2 correspond to $\mathbf{E} \perp C_6$. It can be seen that in these cases the behavior of the impedance is significantly different. In the first case R and X vary approximately like H^2 , and in the second they depend little on H and their values are of the same order as in the anomalous skin effect ($H = 0$). The small deviation of \mathbf{E} from the direction of the open trajectories leads to an abrupt increase of the impedance in the region of strong fields. All these regularities are in qualitative agreement with the conclusions of the theory (see, e.g., (51)) at $\lambda \xi |t_+| \ll 1$. The abrupt angular dependence of the impedance was used to determine the orientation of \mathbf{E} relative to the crystallographic axes. The impedance of the plates with $\mathbf{n} \parallel [10\bar{1}0]$ behaves similarly.

2. The plate-impedance oscillations were investigated by a modulation technique. A signal V_2 at double the modulation frequency was separated in the experiment. The amplitude of the modulation field was set close to the value $0.48\Delta H$ at which the recorded signal reaches a maximum (ΔH is the period of the oscillations). Figure 2 shows plots of

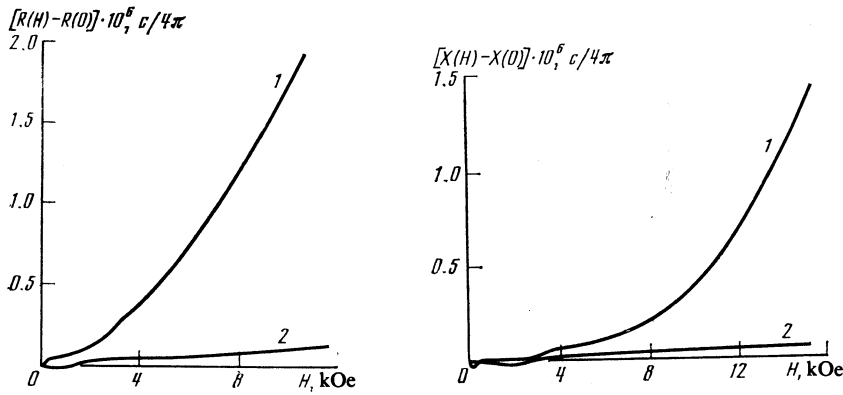


FIG. 1. Surface resistance (a) and reactance (b) of a cadmium plate $d = 1.14$ mm thick as a function of the magnetic field. Frequency 510 kHz, $T = 2$ K, $\mathbf{H} \parallel \mathbf{n} \parallel [11\bar{2}0]$. Curve 1— $\mathbf{E} \parallel C_6$, curve 2— $\mathbf{E} \perp C_6$.

the oscillations in the cases $\mathbf{E} \parallel C_6$ (curve 1) and $\mathbf{E} \perp C_6$ (curve 2). Both plots were obtained at the same gain. It can be seen that when \mathbf{E} is oriented along open trajectories the oscillations have a considerably lower amplitude than at $\mathbf{E} \parallel C_6$ and exist only in the region of relatively weak magnetic fields. At $H > 3$ kOe the difference between the amplitudes exceeds two orders. The oscillations curve 1 have practically a constant period $\Delta H = 70$ Oe ($d = 1.14$ mm), corresponding to a value $(\partial S / \partial p_z)_{ext} = 1.22 \hbar \text{ \AA}^{-1}$. Actually the structure of curve 1 is more complicated: besides the oscillations with the indicated period, it contains also oscillations of much larger period but of smaller amplitude (see subsection 4 below).

The oscillation period for plates with $\mathbf{n} \parallel [10\bar{1}0]$ also corresponds to the value $(\partial S / \partial p_z)_{ext}$ cited above (see Fig. 3). This is evidence that the fundamental oscillations for all samples are connected with the DSCR of the lens electrons, for which C_6 is a rotation axis. This is also confirmed by the fact that when the vector \mathbf{H} is deflected from the normal the period of the oscillations in the hexagonal plane decreases in proportion to the cosine of the angle between \mathbf{H} and \mathbf{n} .

The curves of Figs. 2 and 3 show clearly the oscillation beats. The inclination of the magnetic field in the hexagonal plane has practically no effect on the beat picture. On the contrary, the envelope of the oscillations changes noticeably

when the field is inclined to the lens plane. Thus, for samples with $\mathbf{n} \parallel [11\bar{2}0]$ the beats vanish when \mathbf{H} is deflected from the (0001) plane by about 25° . The positions of some of the nodes and antinodes of the oscillation curves do not depend on the frequency. These data give grounds for assuming that the beats are due to the presence of two close singled-out values of the function $\partial s / \partial p_z$ in a geometry in which the vector \mathbf{H} lies in the plane of the lens. It appears that these values correspond to the limiting points and to the lens section on which the function $\partial s / \partial p_z$ has a maximum.

The necks of the surface-resistance oscillations on the $V_2(H)$ curves corresponding to the orientation $\mathbf{E} \parallel C_6$, marked in Figs. 2 and 3 by a thick arrow, are not nodes of the beats. In contrast to beats, whose position does not depend on f , the position of these necks varies with frequency approximately like $f^{1/2}$. They are located near the field value H_M at which $R(H)$ has a maximum. In accord with the theory, H_M is proportional to $f^{1/2}$. In the vicinity of the point H_M the values of R and X turn out to be close. And it is precisely in this field region that the amplitude of the oscillations of the surface resistance decreases almost to zero, and their phases change smoothly by π . On the contrary, the amplitude of the reactance oscillations near the field H_M reaches a maximum. This behavior of the oscillations is similar to the properties

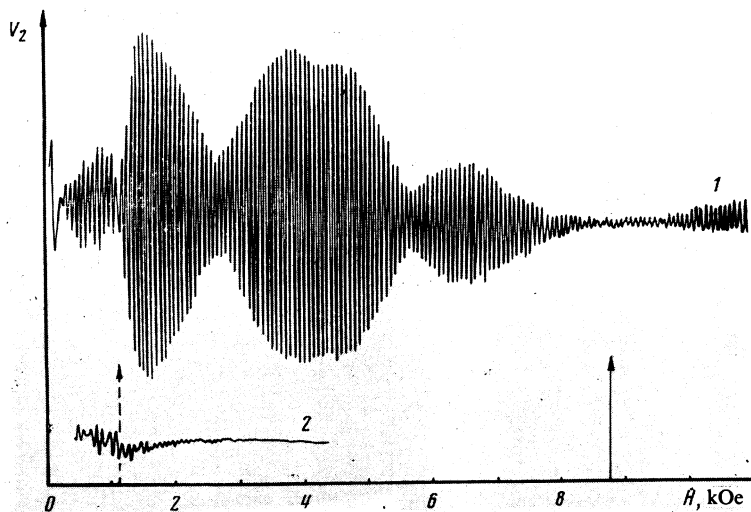


FIG. 2. Oscillations of the surface resistance of a cadmium plate at a polarization of the field \mathbf{E} perpendicular and parallel to the direction of the open trajectories. Thickness $d = 1.14$ mm, $\mathbf{H} \parallel \mathbf{n} \parallel [11\bar{2}0]$, $f = 98$ kHz, $T = 2$ K.

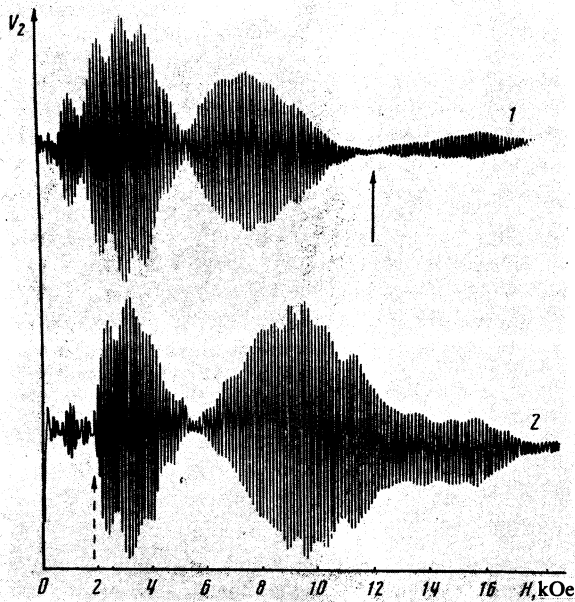


FIG. 3. Oscillations of surface resistance (1) and reactance (2) of a cadmium plate at $\mathbf{H} \parallel \mathbf{n} \parallel [11\bar{2}0]$, $\mathbf{E} \parallel C_6$. Thickness $d = 0.68$ mm, $f = 650$ kHz, $T = 2$.

of the GKO following excitation by a nearly polarized field in the absence of open orbits.⁸

3. On curve 1 of Fig. 2 and on curve 2 of Fig. 3, in the vicinity of the field marked by a dashed arrow, and abrupt increase of the amplitude of the oscillations is observed. These values of H agree well with the doppleron threshold field $H_L = 2.5$ kOe/MHz^{1/3} obtained in Ref. 5. With increasing frequency, the extrema of the oscillations in the narrow region $H > H_L$ shift towards stronger fields. In weaker and in stronger magnetic fields the position of the extrema is independent of frequency with good accuracy. This indicates that the contribution of the doppleron is significant only in a narrow field region above the H_L threshold.

4. Besides the fundamental oscillations connected with the DSCR of the electrons, oscillations with a large period were observed in the $\mathbf{H} \parallel [11\bar{2}0]$ geometry (see Fig. 4). Their maximum amplitude was smaller by at least an order of mag-

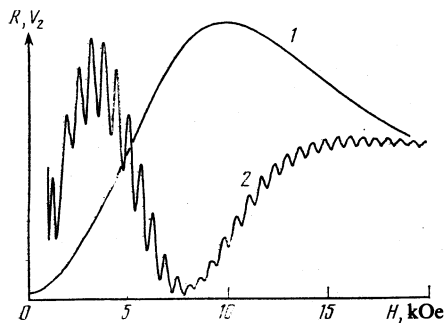


FIG. 4. Surface resistance (1) and its oscillations (2) for a cadmium plate: $d = 1.14$ mm, $\mathbf{n} \parallel [11\bar{2}0]$, $\angle(\mathbf{H}, [11\bar{2}0]) = 5.8^\circ$, $\mathbf{H} \perp C_6$, $f = 104$ kHz, $T = 2$ K.

nitude than the maximum amplitude of the fundamental oscillations. These oscillations could be separated by choosing a field-modulation amplitude such that the fundamental oscillations were suppressed. The long-period oscillations have the largest amplitude in the case $\mathbf{E} \parallel C_6$ and are practically absent in the case $\mathbf{E} \perp C_6$. Their period is constant. They exist at an angle up to 7° between the vector \mathbf{H} and the $[11\bar{2}0]$ axis, and their amplitude varies slowly with the field. Near the maximum of $R(H)$ the amplitude of the oscillations has a minimum as a function of H . These properties of the long-period oscillations allow us to conclude that they are GKO. In the $\mathbf{H} \parallel \mathbf{n} \parallel [10\bar{1}0]$ geometry such oscillations were not observed, but they can be seen for plates with $\mathbf{n} \parallel [10\bar{1}0]$ in an oblique field when \mathbf{H} is close in direction to $[11\bar{2}0]$. A distinguishing feature of the oscillations is the strong anisotropy of their period and amplitude (Fig. 5). The dashed sections of the curves in this figure correspond to the angle region in which beats of the oscillations are observed. Deflection of the vector \mathbf{H} from the hexagonal plane by an angle 2° led to a decrease of the amplitude by approximately 10 times, while the period changed little.

The anisotropy of the oscillations gives grounds for assuming that they are connected with DSCR of the monster holes. The inset of Fig. 5 shows the intersection of the monster with the plane, and the thick lines indicate the proposed regions where the resonant carriers are located. The value of $(\partial S / \partial p_z)_{ext}$ for $\varphi = \varphi_0 = 5.8^\circ$ is $11.0 \hbar \text{ \AA}^{-1}$. The relative change of $(\partial S / \partial p_z)_{ext}$ is described by curve 1 of Fig. 5.

It can thus be seen from the presented results that all the observed oscillations have a maximum amplitude when \mathbf{E} is oriented transverse to the open trajectories. This is in full agreement with main conclusion of the theory.

5. The model used above can be easily modified to describe uncompensated metals. Such a description, however, turns out to be unsatisfactory. The point is that real colli-

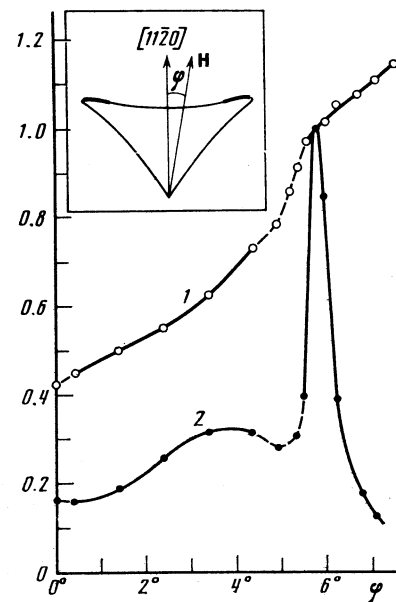


FIG. 5. Dependence of the period (1) and of the maximum amplitude (2) of the long-period oscillations on the angle between the field \mathbf{H} and the $[11\bar{2}0]$ axis in the hexagonal plane. The plots are in relative units.

sionless absorption connected with open orbits leads to a rapid decrease of the oscillation amplitude in a rather narrow interval of H beyond the helicon threshold H_l . In addition, only dopplerons corresponding to the minimum of $\partial S / \partial p_z$ are observed in such metals. These dopplerons appear predominantly in the field region below H_l . In our model, however, owing to the absence of collisionless absorption on the open orbit and owing to the fact that the resonant singularity in the conductivity is pole-like rather than root-like, the maxima of the amplitudes of both the helicon and doppleron oscillations occur in fields greatly exceeding H_l .

In view of the unsuitability of the model, we can use only general considerations. In real metals the conductivity along open trajectories has the same character as under conditions of the anomalous skin effect at $H = 0$. Therefore the corresponding element of the impedance tensor Z_{yy} does not depend on the magnetic field. On the other hand the conductivity transverse to the open trajectories decreases with increasing H , as a result of which the element Z_{xx} is a growing function of the field. It appears that a common property is also the fact that in nonspecular reflection of the electrons the amplitudes of the oscillations in the impedance elements increase together with the smooth parts of the corresponding elements. Thus one should expect the ratio of the oscillating part of Z_{xx} to the oscillating part of Z_{yy} to increase with H . Since helicon and doppleron oscillations in noble metals are observed at $H \parallel [110]$ in relatively weak fields and do not go far beyond the helicon threshold, the ratio $\Delta Z_{xx} / \Delta Z_{yy}$ does not differ greatly from unity. Under these conditions the use of linear polarizations of the exciting field is not effective. It is convenient to choose two elliptic polarizations that differ only in the direction of the field rotation. The major axis should be parallel to the y axis, and the axis ratio must be chosen such that oscillations of a given type are not excited for one of the polarizations. The possibility of such a choice is due to the fact that despite the presence of open orbits the helicon and doppleron propagating in the metal have circular polarization. The ratio of the axes of the exciting field will be called the ellipticity of the oscillations (it must not be confused with the polarization of the corresponding mode). On the basis of the statements made above one can expect the ellipticity of the helicon and doppleron oscillations to decrease with the magnetic field.

The experimental results for silver, shown in Fig. 6, confirm this conclusion. A silver plate 0.811 mm thick with normal $\mathbf{n} \parallel [110]$ was produced by the technology described in Ref. 9. This sample was used earlier in Ref. 10. The polarization of the field of the crossed coils was chosen to match the doppleron. The plots shown in Fig. 6 were obtained for opposite directions of the magnetic field H , with curve $2a$ plotted with a gain 50 times larger than curve $1a$. From a comparison of these curves it follows that the error in the choice of the polarization of the doppleron oscillations does not exceed 1–2%. Practically all the doppleron oscillations lie substantially lower than the helicon threshold. It must therefore be assumed that they are circularly polarized.

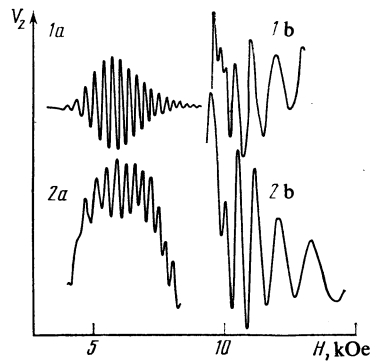


FIG. 6. Oscillations of surface resistance in silver. $H \parallel \mathbf{n} \parallel [110]$, $d = 0.811$ mm, $f = 300$ kHz, $T = 4.2$ K; curves $1a$ and $1b$ correspond to a circular polarization plus, and $2a$ and $2b$ to a circular polarization minus. All the plots were obtained at a field modulation 186 Oe.

Curves $1b$ and $2b$ are continuations of curves $1a$ and $2a$, respectively. The gains for the curves $2b$ and $1b$ are respectively 10 and 100 times larger than for curve $1a$. The oscillations on curve $2b$ are connected with the helicon. Similar oscillations are observed also in the plus polarization (curve $1b$), and their amplitude is 5–10% of the amplitudes of the oscillations on curve $2b$. Since this value exceeds considerably the possible error in the choice of the polarization, it follows that the polarization of the helicon oscillations is not circular. It can be seen here from curves $1b$ and $2b$ that the deviation of the polarization from circular increases with H . By varying the amplitudes and the phases of the voltages on the crossed coils we attempted to choose a polarization such that there would be no helicon oscillations. It turned out that for such value of the magnetic field there exists an amplitude ratio that satisfied this requirement, and this ratio (and hence the oscillation ellipticity) depends on the value of H .

¹I. F. Voloshin, V. G. Skobov, L. M. Fisher, and A. S. Chernov, Zh. Eksp. Teor. Fiz. **86**, 2392 (1981) [Sov. Phys. JETP **53**, 1251 (1981)].

²I. F. Voloshin, V. G. Skobov, L. M. Fisher, and A. S. Chernov, Fiz. Tverd. Tela (Leningrad) **23**, 1721 (1981) [Sov. Phys. Solid State **23**, 1002 (1981)].

³I. F. Voloshin, S. V. Medvedev, V. G. Skobov, L. M. Fisher, and A. S. Chernov, Zh. Eksp. Teor. Fiz. **71**, 1555 (1976) [Sov. Phys. JETP **44**, 814 (1976)].

⁴V. P. Naberezhnykh and A. A. Maryakhin, Phys. Stat. Sol. **20**, 737 (1976).

⁵V. P. Naberezhnykh and T. M. Eremenko, Phys. Stat. Sol. **58**, K175 (1973).

⁶M. Berset, W. M. MacInnes, and R. Hugenin, Helv. Phys. Acta **49**, 695 (1976).

⁷I. F. Voloshin, V. G. Skobov, L. M. Fisher, A. S. Chernov, and V. A. Yudin, Zh. Eksp. Teor. Fiz. **73**, 1884 (1977) [Sov. Phys. JETP **46**, 989 (1977)].

⁸I. F. Voloshin, V. G. Skobov, L. M. Fisher, and A. S. Chernov, Zh. Eksp. Teor. Fiz. **78**, 339 (1980) [Sov. Phys. JETP **51**, 170 (1980)].

⁹V. A. Gasparov, Zh. Eksp. Teor. Fiz. **68**, 2259 (1975) [Sov. Phys. JETP **41**, 1129 (1975)].

¹⁰V. A. Gasparov, L. M. Fisher, and V. A. Yudin, Fiz. Tverd. Tela (Leningrad) **18**, 2716 (1976) [Sov. Phys. Solid State **18**, 1583 (1976)].

Translated by J. G. Adashko